

Microstructuring of the end-surface for silver halide polycrystalline fibers to suppress Fresnel reflection

SONATA ADOMAVIČIŪTĖ-GRABUSOVĖ, 1,2 JONAS HINKEL, 2,3 ISKANDER USENOV,^{2,4} ALEXANDER S. NOVIKOV,^{2,4,*} TATIANA SAKHAROVA, TORSTEN DÖHLER, UTE GEIßLER, 3 ELENA FELIKSBERGER.² AND VIACHESLAV ARTYUSHENKO²

Abstract: Silver halide polycrystalline infrared fibers (PIR) have unique properties such as excellent transmittance in the spectral range from 3 to 17 µm, while also being highly flexible, non-toxic, and non-hygroscopic. They are used in industry and medicine for CO₂-laser power delivery, flexible infrared imaging, and remote process spectroscopy. While PIR fibers possess a quite low attenuation (0.1-0.5 dB/m) in the 8-12 µm range, their total transmittance is limited by significant Fresnel reflections at the fiber end faces due to the high refractive index of silver halide (>2.1). Functionalization of these surfaces with specially designed Anti-Reflective Microstructures (ARMs) enables a striking enhancement of fiber transmittance. In this work, direct imprinting (or embossing) of microstructures to fiber ends and their profiling with a microstructured knife was applied to fabricate such ARMs. The resulting two-dimensional Moth-eye microstructures and one-dimensional microgrooves at the PIR-fiber ends enable to an increase of fiber transmittance in a broadband range of (5-17 µm) as well as to reach up to 20% improvement for PIR-fiber laser cables used for power delivery of CO₂-lasers at 10.6 μm.

© 2021 Optical Society of America under the terms of the OSA Open Access Publishing Agreement

1. Introduction

Polycrystalline infrared (PIR) fibers made by extrusion from solid solutions of silver halides $(AgCl_{1-x}Br_x)$ possess excellent transmission values in the spectral range from 3 to 17 μ m [1,2]. The applications for PIR fibers include flexible power delivery for CO, CO₂ and quantum cascade laser systems [3-5] in addition to mid-infrared (mid-IR) spectroscopy [2], flexible infrared imaging [6,7], and pyrometry [8,9].

While PIR fibers have low intrinsic losses in the mid-IR range, Fresnel reflectance losses at the fiber ends significantly reduce overall transmission due to the high-refractive index contrast between the fiber material ($n_{fiber} \approx 2.15$ for infrared region) and air ($n_{air} = 1$). Data on the refractive index dispersion and the attenuation for AgClBr solid solutions are scarce and in the case of the refractive index not fully consistent (e.g. compare the summarized data in [10] with [11]). Most probably, both depend on the material manufacturing process to some extent. In this paper, we estimated the refractive index dispersion for AgCl_{0.25}Br_{0.75} and AgCl_{0.5}Br_{0.5} compositions used as core and clad of PIR fibers, respectively. This data were used to calculate the optical properties of PIR fibers in the mid-IR range. The refractive index of 2.15 for PIR fibers at wavelengths of 3-16 µm corresponds to Fresnel reflection losses of approximately 13% from one surface. Thus about 25% Fresnel reflection at two surfaces of PIR fiber piece notably

#439904 https://doi.org/10.1364/OME.439904 Journal © 2022 Received 11 Aug 2021; revised 24 Oct 2021; accepted 23 Nov 2021; published 3 Dec 2021

 $^{^{1}}$ Institute of Chemical Physics, Vilnius University, Sauletekio av. 3, LT- 10257 Vilnius, Lithuania

²Art photonics GmbH, Rudower Chaussee 46, 12489 Berlin, Germany

³Technical University of Applied Science Wildau, Hochschulring 1, 15745 Wildau, Germany

⁴Technische Universität Berlin, Institute of Optics and Atomic Physics, Straße des 17. Juni 135, 10623 Berlin, Germany

^{*}an@artphotonics.de

impede high-power delivery for laser radiation. For complex systems that contain multiple PIR fibers, this value is significantly higher and can be estimated as $1 - (1 - R)^k$, where R is a Fresnel coefficient of power reflectance and k is the number of interfaces. For example, PIR fibers are the main component in Attenuated Total Reflectance (ATR)-probes that are used for real-time reaction monitoring in the Chemical, Petrochemical, Atomic, Biopharmaceutical and Food industries [12,13]. ATR probes consist of at least two fibers and thus four interfaces that result in 43% power losses due to Fresnel reflection. Eliminating or reducing these losses would result in a significantly increased signal to noise ratio and improved sensitivity of the probe and thus the whole spectroscopic system. Therefore, improving single-surface transmittance for PIR fibers is very important, especially for laser power delivery and spectroscopic systems.

There are different methods of surface modification to reduce Fresnel reflection losses, and the most used one is thin film coating [14–16]. Despite being the most frequently implemented on various fiber materials and for numerous applications, the anti-reflection thin film shows some drawbacks. Insufficiently wide spectral range for spectroscopy applications and low laser induced threshold for laser optics applications limit the use of fibers treated with anti-reflection coating [17–19]. Moreover, in the case of high-power laser radiation, differences in thermal expansion coefficients of the fiber core, cladding and coating material can lead to cracks in the coating [18]. This, together with the high refractive index of AgClBr fiber, makes the choice of coating material difficult. In addition, the sensitivity of AgClBr material to the heat exposure (above 140 °C) and UV irradiation also limits the number of suitable coating techniques [10]. Furthermore, the softness of the AgClBr makes polishing impossible and the plasticity of the AgClBr material prevents perfect cleavage, at the same time a slicing technique used to prepare the fiber surface still results in non-perfect flatness which leads to a poor coating quality. Nevertheless, there are some examples of using anti-reflection coatings for silver halide fibers in literature [20–22].

An entirely different approach to the reduction of Fresnel reflection is the creation of antireflective microstructures (ARMs). The difference from antireflection coating approach is that an effective refractive index at the fiber surface is created by a sub-wavelength profiled structure [15,23,24]. The best known of the profiled anti-reflective structures is named after its biomimicry, the "moth's eye". These nano-textures create an effective light trap, which theoretically reduces the reflection down to 0.1% [25]. This light trapping effect also occurs in the short wavelength range, where the period of the structure is greater than the wavelength [10]. Profiled anti-reflection structures have some advantages, in particular, they can be made of the substrate material and therefore have a higher mechanical strength and a higher laser-induced damage threshold [26]. They can be designed for a broad spectral and angular range [27]. There are a number of techniques to create ARMs on the optics, e.g. lithography [28,29], laser ablation [29,30], etching [31], molding [32–34], etc. [24,35]. Not all of them are suitable in our case for PIR fiber end faces due to the reasons discussed before. However, the most straightforward and simply implemented ones are a direct imprinting (in some cases also called embossing or stamping), and profiling with a microstructured knife (also called a Special Microstructure Anti-Reflection Treatment (SMART) in [1]). The former allows the fabrication of two-dimensional ARMs on a fiber tip via direct contact with a master plate, while the latter creates one-dimensional grooves by profiling the fiber tip. These structures gradually reduce the refractive index of the fiber surface and allow to obtain a better optical impedance match.

Here, we investigate the surface modification of the polycrystalline silver halide fiber tip using direct imprinting and profiling methods. The possibility of direct formation of ARMs at room temperature (about 22 °C) is demonstrated with respective spectral and profile characterizations. Two methods for ARM formation are demonstrated - imprinting on the PIR fiber end face using a master plate with Moth-eye structure and direct profiling with a microstructured knife that creates microgrooves.

2. Experimental methods

2.1. Computational methods

In order to substantiate the measurements and to gain a deeper understanding of the anti-reflection performance of the produced ARMs, these structures were simulated using the finite difference frequency domain method implemented in COMSOL Multiphysics. The refractive indices used for the simulations were obtained by fitting measurement data (estimated) and a Sellmeier equation for the visible range, both published in [11].

All calculations of transmission were performed using experimental data of the microstructures. The dimensions of the microstructures on the master plate and imprinted fiber ends were measured with a three-dimensional profilometer.

2.2. Profile measurements

To measure profiles of the fiber end faces after modification, the laser confocal optical profilometer VK-X1100 from KEYENCE was used with a 100x objective (NA = 0.8, working distance of 2 mm, nominal resolution of 12 nm in height and 40 nm laterally). The original ARMs and the ones created on the fibers were measured in three randomly chosen spots in different directions obtaining at least three data points in each direction and overall at least 27 data points. Obtained data were averaged and standard deviation was calculated.

2.3. Materials

Imprinting was performed using 0.9 m long polycrystalline fibers with $900/1000 \, \mu m$ core/clad diameters and $AgCl_{0.25}Br_{0.75}/AgCl_{0.5}Br_{0.5}$ core/clad composition (Art Photonics, Germany). A diamond mold plate with anti-reflective Moth-eye structure (Telaztec, USA) was used as a master plate to obtain two-dimensional patterns. One-dimensional profiling was done using a special knife made from a cleaved silicon wafer with grooves. The geometry of the micro grooved one-dimensional silicon knife and two-dimensional Moth-eye microstructures was specifically optimized for high anti-reflectance performance in the range $8-12 \, \mu m$.

Before usage, the master plate was cleaned from previous $AgCl_{1-x}Br_x$ fiber residues. Cleaning was performed by 15 minutes sonication in concentrated hydrochloric acid solution. After that, the master plate was rinsed with ethanol and dried with a nitrogen flow.

2.4. Imprinting of moth-eye microstructures (2D-imprinting)

Moth-eye impress is a two-dimensional (2D) microstructured surface that is embossed on the fiber end faces by using a master plate. During the imprinting experiments, the fiber was secured in the plastic tubing with the fiber ends tightened in the ferrule using a squeeze connector. This squeeze connector allows securing of the fiber inside a ferrule and prevents its movement during the imprinting process.

A setup was built for the imprinting of the Moth-eye ARMs on the fiber end (general scheme is shown in Fig. 1). In the setup, the ferrule is tightened in a special holder and the relative position between the fiber and the master plate can be changed in x, y and z directions using micrometer drives. The master plate was then pressed onto the fiber. Imprinting was performed at room temperature (about $22\,^{\circ}$ C).

2.5. Fiber end face profiling with the microstructured knife (1D-profiling)

The 1D-profiling is the creation of one-dimensional microstructures - grooves and ridges - as a result of shaving (slicing, scraping) with a profiled knife made of a cleaved silicon substrate with grooves. The microstructures on the knife surface were produced using grayscale photolithography. The geometry of these microstructures was approximately trapezoidal-shaped, with parameters,

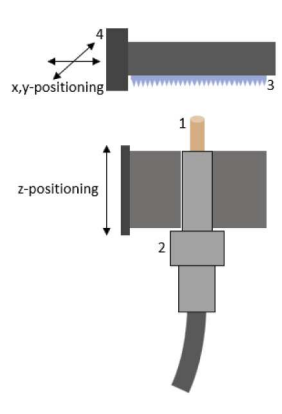


Fig. 1. General scheme of the setup for imprinting of ARMs to the fiber end. Setup parts are indicated by numbers: 1 – fiber; 2 – squeeze connector; 3 – master plate; 4 – holder for a master plate.

shown at Fig. 5. The 1D-profiling was performed by slicing the fiber tip surface with the structured knife edge at room temperature (about 22 °C).

2.6. Temperature and force measurements for 2D-imprinting

As the efficient imprinting of the Moth-eye ARMs on the fiber end depends on the mechanical properties of the material and consequently, on the temperature of the fiber material [36–38], it is necessary to understand the amount of force required for a successful result. As follows, the next setup was built to investigate the temperature influence on the required force for the imprinting process (see Fig. 2). For this, the master plate with Moth-eye structure was fixed on a hot plate (Kyntel, Peru). The fiber was tightly glued inside the ferrule and pressed to the master plate heated from the bottom. Thus the heating of the fiber occured only on the surface in physical contact with the master plate. The temperature of the master plate was measured with a thermocouple. Force was applied by pressing the load cell onto the fiber (moving in z direction) and measured with a load cell. The load cell with the signal amplifier and microcontroller was connected to the computer.

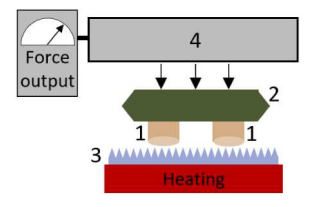


Fig. 2. Experimental setup for force versus temperature measurements. Setup parts are indicated by numbers: 1 – fiber; 2 – fiber capsule; 3 – master plate; 4 - load cell.

2.7. Transmission measurements

For the measurements of fiber performance, two optical setups were used. The first setup contained a CO_2 -laser source with a maximum 10 W output power (Diamond C-40 air-cooled laser GEM 40A Circular, Coherent Inc., USA) and necessary optical components to guide the laser beam and a power meter to measure transmitted power. The second setup used a mid-IR spectrometer (Fourier transform infrared (FTIR) spectrometer ReactIR 1000 with Mercury-Cadmium-Telluride (MCT) detector) to measure changes in transmission over a broad wavelength range. The

measurements of optical power and fiber transmission were performed on the initial fiber and afterwards the same fiber with formed ARMs on its ends. The scheme of the measurements is shown in Fig. 3. As percentages are already used to represent the fiber transmittance, here the improvement in transmittance is presented in terms of relative enhancement in fiber transmission, i.e. the ratio between the transmittance of treated and untreated fiber (also using percentages).

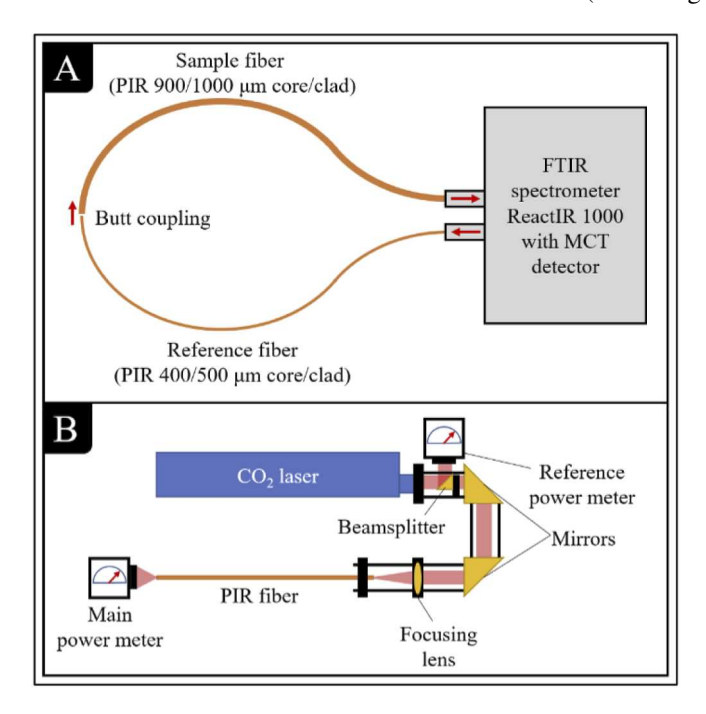


Fig. 3. Scheme of the transmission measurements using a CO_2 -laser for 10.6 μ m wavelength transmission (a) and a FTIR spectrometer for broad wavelength range (b).

3. Results

3.1. Imprinting of the moth-eye microstructures (2D-imprinting)

The best achieved replication of the Moth-eye microstructure, i.e. when the whole fiber end surface area was imprinted and covered by ARMs, was achieved only after the optimisation of the imprinting process. The master Moth-eye plate features a similar structure of truncated cones arranged in a hexagonal array present in the eyes of moths [39,40]. These structures are known to be anti-reflective. Depending on the height (H), period (Λ) and structure size at the top (D) and bottom (B) (Fig. 4), the anti-reflective performance can be shifted from visible light to infrared and mid-IR range [41–43]. Effectively, such structures create a gradually changing refractive index when the wavelength of incident radiation is comparably longer than the dimensions of the structure [44]. For imprinting of the ARMs onto $AgCl_{1-x}Br_x$ fibers we used cone type Moth-eye microstructures fabricated on the diamond plate. Three-dimensional optical profilometer images of the master plate (Fig. 4(a)) revealed a Λ of 3.06 ± 0.18 μ m, the D of 1.05 ± 0.26 μ m, the B of 0.6 ± 0.4 μ m. The H of Moth-eye microstructures was 1.22 ± 0.3 μ m.

After the imprinting of the master structure onto the fiber end face, the negative shape (an inversion of the master plate structure) is left behind. Nevertheless, some discrepancies from the expected inverse structure occur. This is due to mechanical properties of the material, such as stiffness, strength, viscoelasticity, toughness, viscosity, i.e. due to elastic response of the fiber material and insufficient time given for complete material flow [45,46].

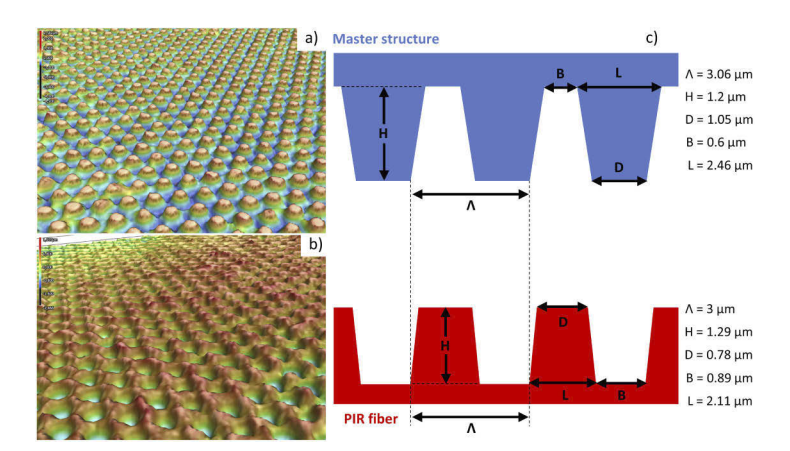


Fig. 4. The 3D profilometer images of the master plate (a) and imprinted fiber surface (b); geometrical parameters of the master plate profile and imprinted fiber end (c).

With our sample, when increase in CO_2 laser transmission by 28.6% was observed, the size D of the imprinted microstructures on the fiber was $0.78\pm0.16~\mu m$ (corresponding to the B of $0.6\pm0.4~\mu m$ on the master plate), $B - 0.89\pm0.14~\mu m$ (corresponding to the D of $1.05\pm0.26~\mu m$ on the master plate), Λ was $3\pm0.09~\mu m$ and B increased to $1.29\pm0.2~\mu m$ (Fig. 4(c)). The increase in the structure height compared with the master structure is unexpected and can be attributed to the sticking of the fiber residues to the master plate after previous imprinting due to more favorable adhesion. Nevertheless, the bottom dimension of Moth-eye ARMs changed from $D = 1.05\pm0.26~\mu m$ to $0.89\pm0.14~\mu m$ when imprinted. Decrease of the size D might also have occurred because of elastic deformation and incomplete imprinting.

All things considered, we expected some decrease in the structure height H due to the incomplete embossing. Because of the limited plasticity, the required time for fiber material to flow under the cavities depends on the material properties and dimensions of the master structure [47]. Nevertheless, a slight increase in structure height was observed experimentally. The size deviation between the individual protrusions and cavities might also have increased because of inhomogeneous pressure on the whole fiber surface – some areas underwent more pressure than others. However, three-dimensional profilometer data reveal apparent microstructures over the entire fiber surface (Fig. 4(b)) after imprinting.

3.2. Fiber surface profiling with a microstructured knife (1D-profiling)

One-dimensional profile of the microstructured knife and related fiber surface pattern are presented in Fig. 5. For this profile, the transmittance for CO_2 -laser increased up to 24% after treatment of both fiber end faces. After the treatment, the fiber surface acquires almost the same structure geometry as the knife edge, but inverted. The resulting height of the structure on the fiber surface profile (approximately 1.75 μ m) is less compared to that on the knife (2.15 μ m). Also, it can be noted that the top corner of the ridges became sharper on the fiber edge, while the groove bottom width or distance between ridges became slightly larger than on the knife. This can be explained by incomplete profiling, i.e. not the whole height of the knife grooves was used.

3.3. Transmission measurements

After the 2D-imprinting of ARMs, the fiber transmission (0.9 m length, $900/1000 \,\mu m$ core/clad diameter) was measured in a broad spectral range using the FTIR spectrometer. After the Moth-eye 2D-imprinting (structure corresponding to Fig. 4), the fiber transmittance increased in the spectral range 5-17 μm (Fig. 6(a)) and decreased in the short wavelength range of 2-5

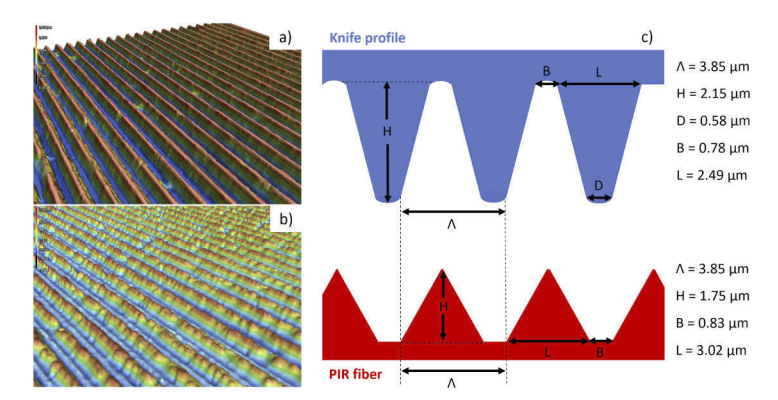


Fig. 5. The 3D profilometer images of grating on the knife edge (a) and microstructured fiber surface after slicing (b); geometrical parameters of the knife profile and fiber end structure after treating (c).

 μ m due to the diffraction. The transmission at 10.6 μ m wavelength increased by 5% after the treatment of one fiber end surface and by 14% after both fiber end surfaces treated, resulting in total transmission increase from 60.5% to 68.8% for two surfaces being treated. Further attempts of Moth-eye imprinting enabled to achieve the transmission increase as high as 25.1% (up to 75.7% on 10.6 μ m wavelength) when both fiber ends were micro-structured (shown in Fig. 6(a) -dashed line). Unfortunately, there was no possibility to measure the corresponding structures with a profilometer. An interesting observation is that after the Moth-eye treatment, the fiber end visually looked almost black (as shown in the Fig. 6 legend inlay).

The transmission increase in in 7.5 μm - 17 μm spectral range (the cut-off wavelength being approximately 7.5 μm) was observed for 1D-profiled fiber surfaces (structure corresponding to Fig. 5). The transmission at 10.6 μm increased by 22.3% from 62.7% to 76.7% after the treatment of both fiber end surfaces (Fig. 6(b)).

The effect of diffraction on the transmittance in short wavelengths range is observed experimentally for both Moth-eye imprinting and profiling of the fiber surface (Fig. 6). The cut-off wavelengths for this effect are different due to the difference of geometrical dimensions for both 1D-profile and 2D Moth-eye structures.

Fibers with 2D-imprinted ARMs were also examined by measuring their transmission with a CO_2 -laser. Data on CO_2 -laser transmission and FTIR measurements for 10.6 μ m from several samples are summarized in Table 1.

The increase of CO_2 -laser transmission is about by 25% (up to 30% in some attempts) at Moth-eye imprinting and about 19%-24% at profiling after both fiber end surfaces treated. The fiber transmittance measurements with FTIR-spectrometer show lower values due to a higher input numerical aperture [27,48], but are in a good agreement with laser transmission results.

Comparison of the 1D-profiling and 2D-imprinting treatment of the fiber shows a similar increase in the transmittance over a broad wavelength range (Fig. 7). At $10.6\,\mu m$ the ratio between the transmissions of treated fiber/initial flat surface is 1.25 and 1.22 for 2D-imprinting and 1D-profiling treatment, respectively. However, with the other 2D-imprinting Moth-eye treatment attempt, the ratio reached only 1.14 (corresponds to Fig. 4). The best results correspond to a single-surface reflectance of 3% (2D-imprinted moth-eye ARM) and 4% (1D-profiling) at $10.6\,\mu m$ wavelength (13% is for untreated surface).

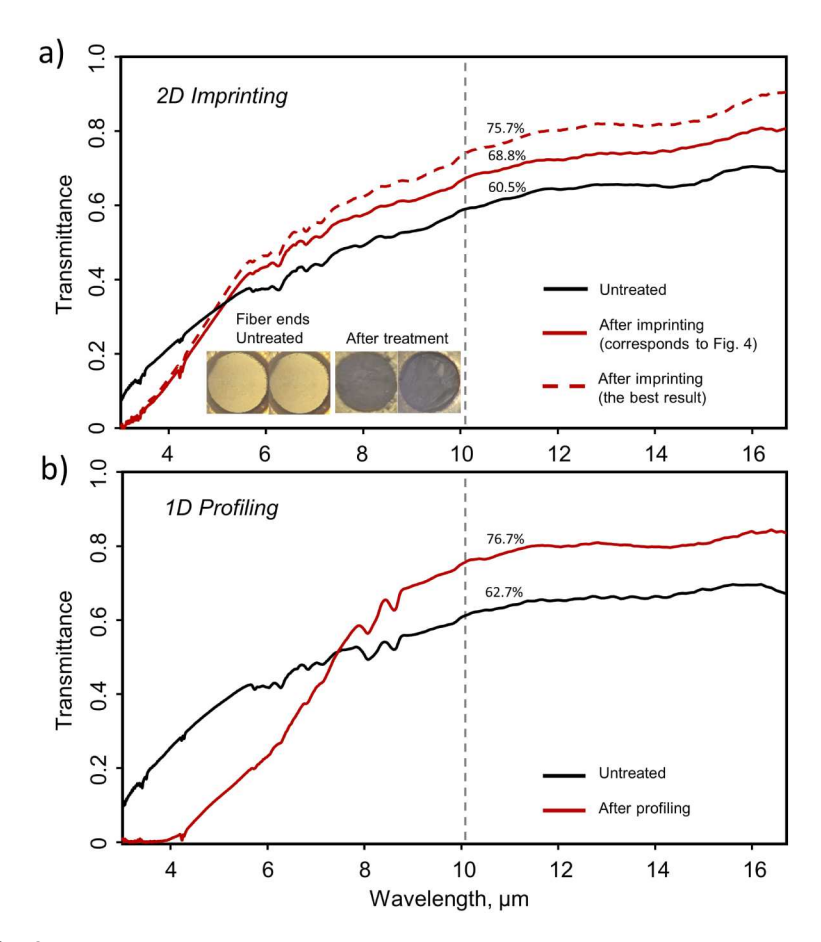


Fig. 6. The measured transmission before and after the 2D Moth-eye imprinting (a) and 1D-profiling (b). In case of Moth-eye treatment (a) dashed line indicates the best result, whereas the solid line shows the result for the structure described at Fig. 4. The legend inlay shows optical microscope pictures of both flat fiber ends (upper), one imprinted fiber end in the input (middle) and both imprinted fiber ends (bottom).

Table 1. Results of ARMs treated fiber transmission at 10.6 μm wavelength measured with CO2-laser and FTIR spectrometer.

Sample No	Treatment type	Increase in CO ₂ -laser transmission, %		Transmission with both ends treated, %	
		One end treated	Both ends treated	CO ₂ -laser	Spectrometer
1	Non-treated	-	-	69	60.5
2	2D imprinted	14	30	90	75.7
3	2D imprinted	13	29	89	73.5
4	2D imprinted	13	29	89	74.4
5	2D imprinted	12	28	88	70.1
6	2D imprinted	10	25	86	68.8
7	2D imprinted	10	25	86	68.9
8	Non-treated	-	-	67	62.7
9	1D profiled	-	24	83	76.7
10	1D profiled	-	19	80	75.2

Research Article

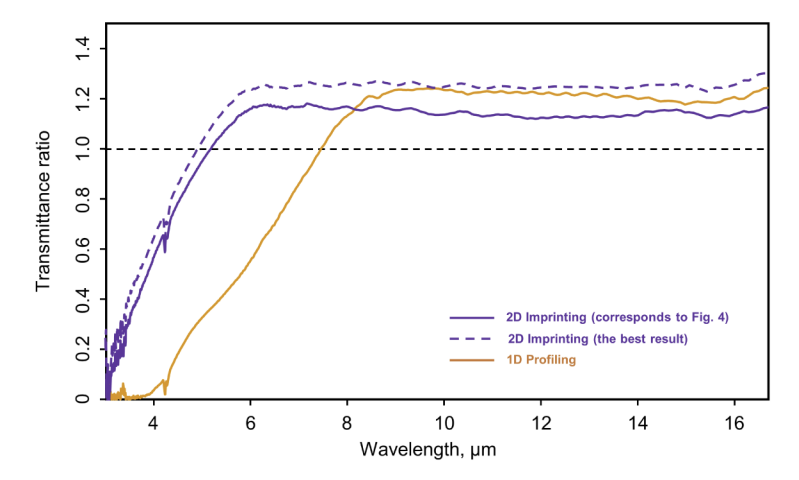


Fig. 7. Comparison of the increase in fiber transmittance ratio for 2D-imprinted Moth-eye microstructures and 1D profiled grooves on both fiber ends.

3.4. Transmission calculation

The refractive indices used for the simulations are obtained by fitting measurement data (estimated) and a Sellmeier equation for the visible range, both published in [11]. For the input function of the fit, a known Sellmeier equation for the component silver chloride, published in [49] was used (Fig. 8). In the fitted function (1) the wavelength λ is given in micrometers.

$$n_{AgCl_{0.25}:AgBr_{0.75}}(\lambda) = \sqrt{4.66 + \frac{78 \cdot 10^{-3}}{\lambda^2 - 32.4 \cdot 10^{-3}} - 1.93 \cdot 10^{-3} \cdot \lambda^2 + 4 \cdot 10^{-6} \cdot \lambda^4}$$
 (1)

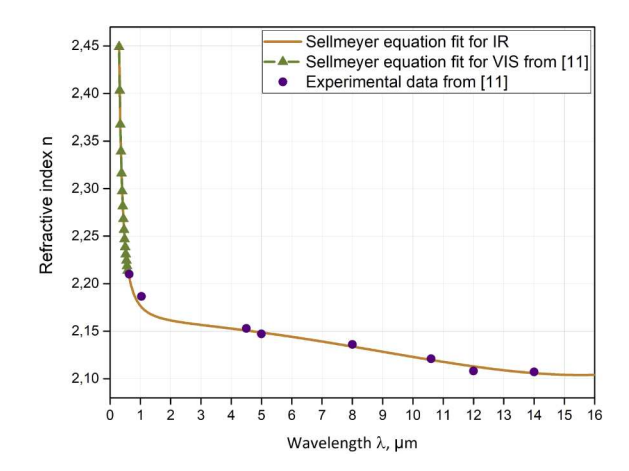


Fig. 8. Sellmeier equation fitted for PIR fiber core material using data obtained from [11] and the Sellmeier equation from [49] as an input function.

Transmission calculations were performed for Moth-eye and groove structures with geometry and sizes specified in Fig. 4 and Fig. 5. According to computational results for Moth-eye ARM treatment (2D-imprinting), increase in the transmission due to anti-reflective contribution occurs in a wide range of wavelengths from 5 μ m to 16 μ m (Fig. 9(a)). The reflection from the single plain air/fiber interface diminishes the transmission to $\approx 87\%$ as calculated from the Fresnel

equations. Whereas, when the ideal Moth-eye ARMs based on the mold geometry are imprinted on the plain fiber end, the single surface transmission at 10.6 μm wavelength increases to 92.5%. When the incident wavelength is close to the dimensions of an ideal Moth-eye ARM ($\Lambda \approx 3~\mu m$), the anti-reflective performance is not noticeable anymore. Because of this effect, the transmission of the radiation is suppressed due to the diffraction in the range of 3-5 μm . Nevertheless, the simulations based on the geometry of experimentally obtained structures after imprinting show that reduced reflection should lead to 93% transmission at 10.6 μm wavelength.

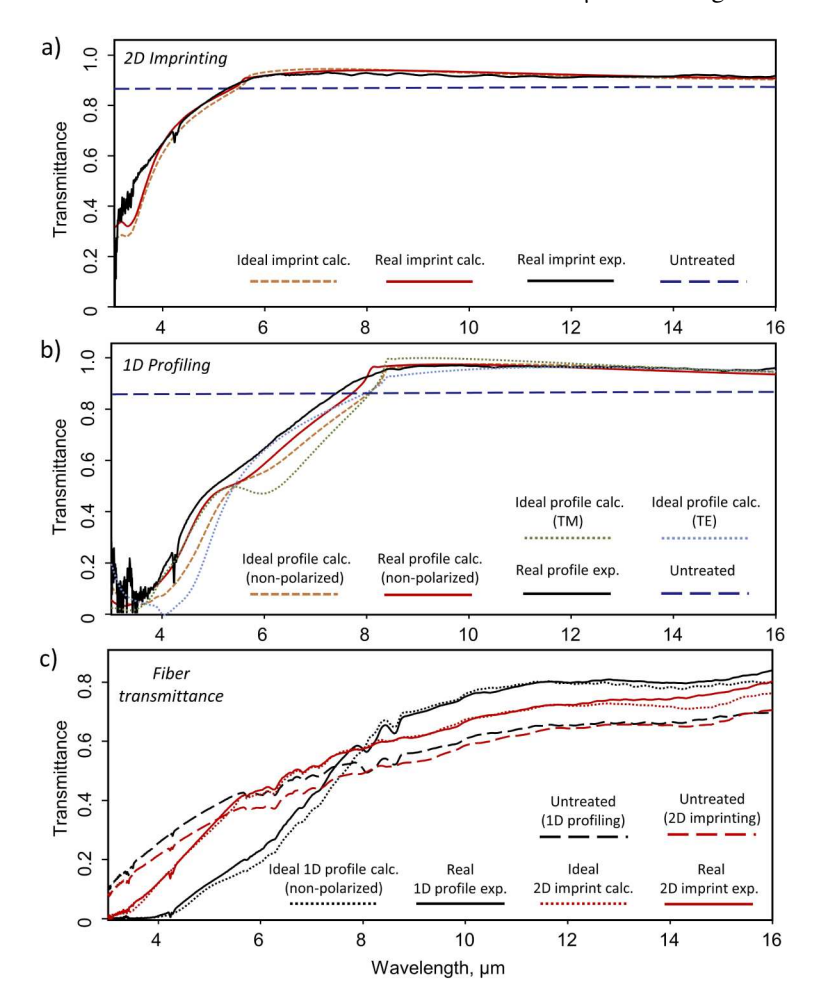


Fig. 9. Comparison between the calculated (calc.) and experimental (exp.) performances of the 1D-profiling and 2D-imprinting, in accordance with data from Fig. 4 and Fig. 5. A) Single surface transmittance of 2D-imprinted fiber tip with Moth-eye ARMs. B) Single surface transmittance of 1D-profiled fiber tip. C) Calculated and measured fiber transmittance in case of treatment of both fiber end faces. Used fibers are PIR fibers with 0.9 m length and $900/1000~\mu m$ core/clad diameters. "Ideal" imprint and profile refer to the inverted structures from the master plate and knife, respectively. "Real" imprint and profile refer to the structures measured on the profilometer.

Similar results were observed with the one-dimensional groove simulations (1D-profiling, Fig. 9(b)). A transmission of 97.4% for $10.6~\mu m$ should be achieved after a perfect treatment (when an ideal inverted structure is attained on the fiber using the knife profile described in Fig. 5). Overall, simulated transmittance for groove ARMs is slightly better than that for the

Moth-eye ARMs, though the cut-off wavelength is higher, providing a more narrow anti-reflective range. For the groove microstructures, the high transmittance is achieved in the range 8-17 μm.

The simulated transmission of single treated fiber surface was compared with the experimental results (Fig. 9(a, b)). For this purpose, an internal attenuation from the raw transmission data of the fiber was excluded and the transmission of single ARMs treated air/fiber interface was evaluated. The obtained experimental results correspond well to the simulations. Nevertheless, transmission values observed in the short wavelength range were better than expected. Although it is not clear yet, this improved transmittance could be explained by neglected interaction between the diffracted radiation and the fiber material. Generally, the transmission losses in the polycrystalline fibers at shorter wavelengths are caused by complex interactions between the Rayleigh-Gans scattering from the micro-grains at the fiber structure and Brillouin scattering, resulting in a λ^{-2} dependency [10,25]. The possible interaction between the short wavelength radiation (approximately 6 μ m and shorter) passing through the ARM treated fiber surface and the micro-grains of the fiber material could be the reason for the improved transmission in the short wavelength range observed in the experiments. Such interaction was not accounted for when experimental single ARMs were evaluated.

The transmittance of the whole 0.9 m length fiber was simulated for the cases of the ideal Moth-eye and ideal grooved ARMs obtained by imprinting/profiling the fiber, i.e. the ARMs on the fiber tips are inverted ARMs from the master plate/knife. The simulated transmittance is compared to the experimentally obtained spectra in Fig. 9(c). Experimental transmission for the used fiber with flat ends is 60.5% (in case of 2D-imprinting) - 62.7% (in case of 1D profiling) at $10.6 \,\mu m$. If the Moth-eye structure obtained by imprinting would be on both fiber ends instead of the flat ends, the transmission would reach 69%. The experimentally obtained value - 68.8% is similar to the expected one. The simulated transmission for the groove ARMs obtained by profiling the fiber should also be similar to the one obtained experimentally and reach 77.9% (experimentally obtained value is 76.7%). In this way, the transmission should increase by 14% after the Moth-eye imprinting (experimentally observed increase is 14%) and by 24% after profiling both ends of the fiber (experimental increase - 22%).

3.5. Temperature and force measurements for 2D-imprinting

The 2D-imprinting described above was performed at room temperature (about 22 $^{\circ}$ C). However, it was found that the force required for imprinting the whole fiber (with 900/1000 μ m core/clad diameters) surface area, i.e. with maximum surface coverage efficiency, can be reduced if the process is performed under higher temperatures. When the heated master plate gets in contact with the fiber end face, the temperature of the fiber end increases that leads to increased plasticity of the fiber material. According to our results, the force needed for imprinting of the whole fiber end area decreased from 90 N at room temperature (about 22 $^{\circ}$ C) to approximately 45 N when the master plate heated to 150-200 $^{\circ}$ C.

4. Discussion

1D-profiling and Moth-eye ARMs treatments lead to similar transmittance improvement of polycrystalline optical fiber in the spectral range 7.5 - 17 μm (see Fig. 7). The main difference is that the resulting transmission increase starts from about 5 μm for Moth-eye ARMs and from 7.5 μm for profiling treatment. The dependency of cut-off wavelength and the amount of reflected radiation on the microstructure dimensions (height, period, top and bottom width) is complex [50,51]. For the Moth-eye ordered microstructures, the height of the relief affects how much the reflectance is suppressed. But the cut-off wavelength does not depend on the height, only on the period. The reduction of the period results in a shift of the cut-off wavelength into the range of shorter wavelengths [30,44,51].

The profilometric measurements show that the resulting geometrical dimensions of the fiber surface profile are different from the surfaces of the profiled knife edge or the moth-eye master plate. This is due to the low plasticity of the fiber material that also tends to stick to the master plate or microstructured knife during the treatment. For further improvement in replicating of ARMs on the fiber surface by embossing technique, an increase in pressure and temperature will be attempted. The higher loading at the contact of the fiber end and master plate should lead to better replication of the microstructures. Moreover, higher temperatures should soften the fiber material and allow to reduce the required force. However, PIR fibers should avoid being heated for a prolonged period of time as it leads to substantial grain growth and increased optical losses [10,26]. Thus, the embossing process will be further optimised. In case of 1D-profiling we believe that the quality of 1D-profiled surface on fiber end face is mainly determined by the silicon knife quality. Thus, for the improvement in the profiling process, the importance to the quality of silicon knives and the whole cutting arrangement should be paid.

While producing one-dimensional structures with 1D-profiling is more cost-effective and simpler, their transmittance is polarisation dependent [52,53] with accordance to our calculations. Of course, in case of non-polarised radiation (for example, in spectroscopy) this property does not produce a notable effect. The 2D-imprinting technique allows the production of 2D gratings with the advantage of polarisation-independent transmittance. This method is more advanced, requires an application of force and temperature to the master plate and needs to be done more accurately and precisely to achieve a good imprint on the fiber end face. In addition, master plates with 2D anti-reflective "moth-eye" structure are much more expensive in comparison to 1D grating used in the previous method. The contamination of the master plate with the polycrystalline fiber material is another problem which leads to reducing the quality of the resulting structure on the fiber end face. The cleaning of the master plate is possible with a method described above, however, it is difficult to get rid of all contaminants because of the fine relief of the structure.

Another significant problem during the imprinting is that usually it is very hard to cleave the fiber end face perfectly perpendicular to the fiber axis. It leads to incomplete physical contact between fiber and master plate during the embossing and results in a non-uniform covering of the ARM structure over the fiber end face.

Despite the problems described above, thermomechanical imprinting and 1D-profiling remain the most straightforward method of fabricating ARMs on the fiber end face.

5. Conclusion

Simple and straightforward methods to suppress Fresnel reflection and increase the transmittance of $AgCl_{1-x}Br_x$ fibers (in a broad spectral range and at CO_2 -laser radiation wavelength, particularly) have been proposed and investigated. Both of these treatments were implemented at room temperature. The shaving of the fiber end with a profiled silicon knife produces one-dimensional anti-reflective grating. Another method is the imprinting of a two-dimensional so called Moth-eye microstructured master plate onto the fiber end face. The theoretical reducing of Fresnel reflection for two structures has been calculated, the experimental results are in a good agreement with calculated values. The transmission spectra of treated optical fibers in the spectral range from 3 μ m to 17 μ m show the effect of diffraction at the surface microstructure on the fiber transmission. The significant transmission increase has been measured in the spectral range from 7 to 17 μ m. Measurement with CO_2 -laser (10.6 μ m wavelength) showed the transmission increase by 25-30% for both fiber surfaces treated. The advantage of 1D-profiling technique is the availability and relatively low cost whereas 2D-imprinting is more promising for broadband anti-reflection treatment with polarisation independence.

Disclosures. The authors declare no conflicts of interest.

Data availability. Data underlying the results presented in this paper are available from the authors upon reasonable request.

References

- V. Artyushenko, A. Bocharnikov, T. Sakharova, and I. Usenov, "Mid-infrared fiber optics for 1 18 μm range," Opt. Photonik 9(4), 35–39 (2014).
- A. Yuzhakova, A. Lvov, D. Salimgareev, A. Korsakov, and L. Zhukova, "Infrared silver halide fiber for medicine application," in 2020 Ural Symposium on Biomedical Engineering, Radioelectronics and Information Technology (USBEREIT) (2020), pp. 0136–0138.
- 3. L. N. Butvina, A. G. Okhrimchuk, A. L. Butvina, E. M. Dianov, N. V. Lichkova, and V. N. Zagorodnev, "Low loss micro and nano structured single mode crystalline fibers for 5-15 μm," in *Advances in Optical Materials* (Optical Society of America, 2011), p. AIThD4.
- S. Israeli and A. Katzir, "Optical losses of AgClBr crystals and fibers in the middle infrared," Opt. Mater. 33(11), 1825–1828 (2011).
- L. N. Butvina, E. M. Dianov, N. V. Lichkova, V. N. Zavgorodnev, and L. Kuepper, "Crystalline silver halide fibers with optical losses lower than 50 dB/km in broad IR region," in *Infrared Optical Fibers and Their Applications*, vol. 3849 M. Saad and J. A. Harrington, eds., International Society for Optics and Photonics (SPIE, 1999), pp. 181–188.
- E. Korsakova, S. Markham, A. Mani, C. Silien, J. Bauer, S. Tofail, L. Zhukova, and A. Korsakov, "MIR imaging bundles of ordered silver halide polycrystalline fibres for thermal transmission and imaging," J. Therm. Anal. Calorim. 142(1), 245–253 (2020).
- S. Delbeck, B. Schmitz, A. Nabers, K. Gerwert, A. Habermehl, U. Lemmer, and H. M. Heise, "Applications of tapered flat silver halide fibers chemically modified by 12-mercaptododecanoic acid NHS ester for infrared biospectroscopy with prospects for medical diagnostics," in *Optical Fibers and Sensors for Medical Diagnostics and Treatment Applications XIX*, vol. 10872 I. Gannot, ed., International Society for Optics and Photonics (SPIE, 2019), pp. 141–151.
- S. Sade, O. Eyal, V. Scharf, and A. Katzir, "Fiber-optic infrared radiometer for accurate temperature measurements," Appl. Opt. 41(10), 1908–1914 (2002).
- 9. B. Lee, W. J. Yoo, D. H. Cho, K. W. Jang, S.-C. Chung, and G.-R. Tack, "Low-temperature radiometric measurements using a silver halide optical fiber and infrared optical devices," Opt. Rev. 14(5), 355–357 (2007).
- 10. J. A. Harrington, Infrared Fibers and their Applications (SPIE-International Society for Optical Engineering, 2003).
- 11. A. S. Korsakov, D. S. Vrublevsky, A. E. Lvov, and L. V. Zhukova, "Refractive index dispersion of $AgCl_1 xBr_x$; $(0 \le x \le 1)$ and $Ag_1 xTl_xBr_1 xI_x$; $(0 \le x \le 0.05)$," Opt. Mater. **64**, 40–46 (2017).
- A. Bogomolov, M. Heßling, U. Wenzel, S. Princz, T. Hellmuth, M. J. B. Bernal, T. Sakharova, I. Usenov, V. Artyushenko, and H. Meyer, "Development and testing of mid-infrared sensors for in-line process monitoring in biotechnology," Sens. Actuators, B 221, 1601–1610 (2015).
- 13. A. Bogomolov, "Developing multisensory approach to the optical spectral analysis," Sensors 21(10), 3541 (2021).
- 14. Y. Matsuoka, S. Mathonnèire, S. Peters, and W. T. Masselink, "Broadband multilayer anti-reflection coating for mid-infrared range from 7 µm to 12 µm," Appl. Opt. 57(7), 1645–1649 (2018).
- H. K. Raut, V. A. Ganesh, A. S. Nair, and S. Ramakrishna, "Anti-reflective coatings: a critical, in-depth review," Energy Environ. Sci. 4(10), 3779–3804 (2011).
- K. C. Krogman, T. Druffel, and M. K. Sunkara, "Anti-reflective optical coatings incorporating nanoparticles," Nanotechnology 16(7), S338–S343 (2005).
- B. Mangote, L. Gallais, M. Commandré, M. Mende, L. Jensen, H. Ehlers, M. Jupé, D. Ristau, A. Melninkaitis, J. Mirauskas, V. Sirutkaitis, S. Kičas, T. Tolenis, and R. Drazdys, "Femtosecond laser damage resistance of oxide and mixture oxide optical coatings," Opt. Lett. 37(9), 1478–1480 (2012).
- A. Sincore, J. Cook, F. Tan, A. E. Halawany, A. Riggins, S. McDaniel, G. Cook, D. V. Martyshkin, V. V. Fedorov, S. B. Mirov, L. Shah, A. F. Abouraddy, M. C. Richardson, and K. L. Schepler, "High power single-mode delivery of mid-infrared sources through chalcogenide fiber," Opt. Express 26(6), 7313–7323 (2018).
- J. Sun, X. Cui, C. Zhang, C. Zhang, R. Ding, and Y. Xu, "A broadband antireflective coating based on a double-layer system containing mesoporous silica and nanoporous silica," J. Mater. Chem. C 3(27), 7187–7194 (2015).
- L. Nagli, A. German, A. Katzir, J. Tschepe, V. Prapavat, H.-G. Eberle, and G. J. Mueller, "Optical catheters based on silver halide infrared fibers," in *Medical and Fiber Optic Sensors and Delivery Systems*, vol. 2631 N. I. Croitoru, M. Miyagi, G. Orellana, A. V. Scheggi, and H. J. C. M. Sterenborg, eds., International Society for Optics and Photonics (SPIE, 1995), pp. 208–215.
- V. N. Glebov, P. G. Leonov, A. M. Malyutin, and V. P. Yakunin, "Protective antireflection coatings for optical IR fibers based on silver halogenides," in *Seventh International Conference on Laser and Laser-Information Technologies*, vol. 4644 V. Y. Panchenko and V. S. Golubev, eds., International Society for Optics and Photonics (SPIE, 2002), pp. 363–365
- O. Wallner, V. G. Artjuschenko, and R. Flatscher, "Development of silver-halide single-mode fibers for modal filtering in the mid-infrared," in *New Frontiers in Stellar Interferometry*, vol. 5491 W. A. Traub, ed., International Society for Optics and Photonics (SPIE, 2004), pp. 636–646.
- 23. Z. Han, Z. Wang, X. Feng, B. Li, Z. Mu, J. Zhang, S. Niu, and L. Ren, "Antireflective surface inspired from biology: A review," Biosurface and Biotribology 2(4), 137–150 (2016).
- 24. D. S. Hobbs and B. D. MacLeod, "Design, fabrication, and measured performance of anti-reflecting surface textures in infrared transmitting materials," in *Window and Dome Technologies and Materials IX*, vol. 5786 R. W. Tustison, ed., International Society for Optics and Photonics (SPIE, 2005), pp. 349–364.
- 25. J. Sanghera and I. D. Aggarwal, Infrared Fiber Optics (CRC Press, 1998).

- D. Bunimovich, S. Shalem, and A. Katzir, "Effects of thermal treatment on the infrared transmission of polycrystalline silver halide fibers," Appl. Opt. 36(1), 285–290 (1997).
- I. R. Lewis and H. Edwards, Handbook of Raman Spectroscopy: From the Research Laboratory to the Process Line (CRC press, 2001).
- 28. D. S. Hobbs, B. D. McLeod, A. F. Kelsey, M. A. Leclerc, and E. S. III, "Automated-interference-lithography-based systems for generation of submicron-feature size patterns," in *Micromachine Technology for Diffractive and Holographic Optics*, vol. 3879 S. H. Lee and J. A. Cox, eds., International Society for Optics and Photonics (SPIE, 1999), pp. 124–135.
- Y. Fu, M. Soldera, W. Wang, B. Voisiat, and A. F. Lasagni, "Picosecond laser interference patterning of periodical micro-architectures on metallic molds for hot embossing," Materials 12(20), 3409 (2019).
- 30. M. K. Tarabrin, A. A. Bushunov, A. A. Teslenko, T. Sakharova, J. Hinkel, I. Usenov, T. Döhler, U. Geißler, V. Artyushenko, and V. A. Lazarev, "Fabrication of an antireflection microstructure on AgClBr polycrystalline fiber by single pulse femtosecond laser ablation," Opt. Mater. Express 11(2), 487–496 (2021).
- 31. D. S. Hobbs, B. D. MacLeod, A. D. Manni, and S. M. Consoles, "Pulsed laser damage resistance of nano-structured polarizers for 1064nm," in *Laser-Induced Damage in Optical Materials 2018: 50th Anniversary Conference*, vol. 10805 C. W. Carr, G. J. Exarhos, V. E. Gruzdev, D. Ristau, and M. Soileau, eds., International Society for Optics and Photonics (SPIE, 2018), pp. 159–170.
- 32. K. Yamada, M. Umetani, T. Tamura, Y. Tanaka, and J. Nishii, "Formation of antireflective structure on the surface of optical glass by molding," in *Advanced Fabrication Technologies for Micro/Nano Optics and Photonics*, vol. 6883 T. J. Suleski, W. V. Schoenfeld, and J. J. Wang, eds., International Society for Optics and Photonics (SPIE, 2008), pp. 23–30.
- 33. G. Du, Q. Yang, F. Chen, H. Liu, Z. Deng, H. Bian, S. He, J. Si, X. Meng, and X. Hou, "Direct fabrication of seamless roller molds with gapless and shaped-controlled concave microlens arrays," Opt. Lett. 37(21), 4404–4406 (2012).
- A. Rank, V. Lang, and A. F. Lasagni, "High-speed roll-to-roll hot embossing of micrometer and sub micrometer structures using seamless direct laser interference patterning treated sleeves," Adv. Eng. Mater. 19(11), 1700201 (2017).
- 35. A. A. Bushunov, M. K. Tarabrin, and V. A. Lazarev, "Review of surface modification technologies for mid-infrared antireflection microstructures fabrication," Laser Photonics Rev. 15(5), 2000202 (2021).
- A. Jacobo-Martín, M. Rueda, J. J. Hernández, I. Navarro-Baena, M. A. Monclús, J. M. Molina-Aldareguia, and I. Rodríguez, "Bioinspired antireflective flexible films with optimized mechanical resistance fabricated by roll to roll thermal nanoimprint," Sci. Rep. 11(1), 2419 (2021).
- 37. J. Sanghera, C. Florea, L. Busse, B. Shaw, F. Miklos, and I. Aggarwal, "Reduced Fresnel losses in chalcogenide fibers by using anti-reflective surface structures on fiber end faces," Opt. Express 18(25), 26760–26768 (2010).
- 38. M. R. Lotz, C. R. Petersen, C. Markos, O. Bang, M. H. Jakobsen, and R. Taboryski, "Direct nanoimprinting of moth-eye structures in chalcogenide glass for broadband antireflection in the mid-infrared," Optica **5**(5), 557–563 (2018)
- 39. A. R. Parker and H. E. Townley, "Biomimetics of photonic nanostructures," Nat. Nanotechnol. 2(6), 347-353 (2007).
- S. Wilson and M. Hutley, "The optical properties of 'moth eye' antireflection surfaces," Opt. Acta 29(7), 993–1009 (1982).
- A. A. Bushunov, M. K. Tarabrin, V. A. Lazarev, V. E. Karasik, Y. V. Korostelin, M. P. Frolov, Y. K. Skasyrsky, and V. I. Kozlovsky, "Fabrication of anti-reflective microstructures on chalcogenide crystals by femtosecond laser ablation," Opt. Mater. Express 9(4), 1689–1697 (2019).
- D. S. Hobbs, "Laser damage threshold measurements of anti-reflection microstructures operating in the near UV and mid-infrared," *Laser-Induced Damage in Optical Materials: 2010*, vol. 7842 G. J. Exarhos, V. E. Gruzdev, J. A. Menapace, D. Ristau, and M. J. Soileau, eds., International Society for Optics and Photonics (SPIE, 2010), pp. 509–521.
- 43. B. D. MacLeod and D. S. Hobbs, "Long life, high performance anti-reflection treatment for HgCdTe infrared focal plane arrays," *Infrared Technology and Applications XXXIV*, vol. 6940 B. F. Andresen, G. F. Fulop, and P. R. Norton, eds., International Society for Optics and Photonics (SPIE, 2008), pp. 318–333.
- 44. S. A. Boden and D. M. Bagnall, Moth-eye antireflective structures (Springer, 2012).
- L. Heyderman, H. Schift, C. David, J. Gobrecht, and T. Schweizer, "Flow behaviour of thin polymer films used for hot embossing lithography," Microelectron. Eng. 54(3-4), 229–245 (2000).
- 46. N. Bogdanski, M. Wissen, S. Möllenbeck, and H.-C. Scheer, "Structure size dependent recovery of thin polystyrene layers in thermal imprint lithography," Microelectron. Eng. **84**(5-8), 860–863 (2007).
- 47. H. Schift and A. Kristensen, Nanoimprint Lithography (Springer Berlin Heidelberg, 2007), pp. 239-278.
- 48. O. Stevens, I. E. I. Petterson, J. C. Day, and N. Stone, "Developing fibre optic Raman probes for applications in clinical spectroscopy," Chem. Soc. Rev. 45(7), 1919–1934 (2016).
- L. W. Tilton, E. K. Plyler, and R. E. Stephens, "Refractive index of silver chloride for visible and infra-red radiant energy*," J. Opt. Soc. Am. 40(8), 540–543 (1950).
- K. Han and C.-H. Chang, "Numerical Modeling of sub-wavelength anti-reflective structures for solar module applications," Nanomaterials 4(1), 87–128 (2014).
- 51. R. J. Weiblen, C. R. Menyuk, L. E. Busse, L. B. Shaw, J. S. Sanghera, and I. D. Aggarwal, "Optimized moth-eye anti-reflective structures for As₂S₃ chalcogenide optical fibers," Opt. Express 24(10), 10172–10187 (2016).

- 52. Y. Yang, S.-C. Liu, Y. Wang, M. Long, C.-M. Dai, S. Chen, B. Zhang, Z. Sun, Z. Sun, C. Hu, S. Zhang, L. Tong, G. Zhang, D.-J. Xue, and J.-S. Hu, "In-plane optical anisotropy of low-symmetry 2D GeSe," Adv. Opt. Mater. 7(4), 1801311 (2019).
- 53. J. Zheng, Z.-C. Ye, N.-L. Sun, R. Zhang, Z.-M. Sheng, H.-P. D. Shieh, and J. Zhang, "Highly anisotropic metasurface: a polarized beam splitter and hologram," Sci. Rep. 4(1), 6491 (2014).